Wavelength scaling of strong-field Rydberg-state excitation: Toward an effective *S*-matrix theory

SongPo Xu,[1,*] MingQing Liu,[2,*] Wei Quan,[1,7,†] XiaoPeng Yi,[3] ShiLin Hu,[4] LiBin Zheng,[1,7] ZhiQiang Wang,[1] Meng Zhao,[1,7] ShaoGang Yu,[1] RenPing Sun,[1] YanLan Wang,[1,7] LinQiang Hua,[1,7] XuanYang Lai,[1,7] Wilhelm Becker,[5] Jing Chen,[3,6,‡] and XiaoJun Liu[1,7,§]

[1]*State Key Laboratory of Magnetic Resonance and Atomic and Molecular Physics, Wuhan Institute of Physics and Mathematics, Innovation Academy for Precision Measurement Science and Technology, Chinese Academy of Sciences, Wuhan 430071, China*

[2]*College of Physics and Optoelectronic Engineering, Shenzhen University, Shenzhen 518060, China*

[3]*Institute of Applied Physics and Computational Mathematics, P.O. Box 8009, Beijing 100088, China*

[4]*Guangdong Provincial Key Laboratory of Quantum Metrology and Sensing School of Physics and Astronomy, Sun Yat-Sen University (Zhuhai Campus), Zhuhai 519082, China*

[5]*Max-Born-Institut, Max-Born-Strasse 2a, 12489 Berlin, Germany*

[6]*Center for Advanced Material Diagnostic Technology, College of Engineering Physics, Shenzhen Technology University, Shenzhen 518118, China*

[7]*School of Physical Sciences, University of Chinese Academy of Sciences, Beijing 100049, China*

(Received 31 March 2022; revised 12 November 2022; accepted 21 November 2022; published 20 December 2022)

S-matrix theory and the Born expansion, the lowest-order term of which is known as the "strong-field approximation" (SFA), play an indispensable role in our understanding of atomic and molecular processes in intense laser fields. Most phenomena in this field are reproduced by the first two terms of the Born series. However, for a long-range potential such as the Coulomb potential, the second-order term may be larger than the SFA term, raising the problem of the convergence of the Born series. By simultaneously measuring and simulating ionization and Rydberg-state excitation of an argon atom subject to a strong laser field for various wavelengths, we demonstrate that the wavelength scaling law of the measured ratio of Ar^* over Ar^+ and the period of its oscillation with respect to the laser intensity can be well reproduced by the second-order term of the *S*-matrix expansion in terms of the Coulomb potential, but not by the lowest-order (SFA) term. We conjecture that the second-order term of the *S*-matrix expansion may provide an effective theory for the intense-laser–atom interaction.

DOI: 10.1103/PhysRevA.106.063106

I. INTRODUCTION

S-matrix theory provides an efficient and physically appealing theoretical tool for the study of the atomic and molecular dynamics in intense laser fields [1–4]. For a given process, its *S*-matrix amplitude is usually expanded into the Born series in powers of the interaction between the active electron and its binding or scattering potential. Its lowest-order term, which incorporates no interaction between the liberated electron and the potential, is referred to as the strong-field approximation (SFA) [1–3]. The next-order term describes exactly one such interaction (see, e.g., Ref. [4]), and each subsequent higher-order term allows for one additional interaction. Each term exactly accounts for the laser field. Naturally, the problem of the convergence of the Born expansion has come up [3,5–7]. Here, we consider Rydberg-state excitation (RSE) of ground-state argon by an intense laser field. We confront measurements of the intensity and wavelength dependence of the RSE yield with the results of a Born series expansion. We conjecture that, regardless of the convergence of the series, the second-order term affords an effective theory.

For a short-range potential with an interaction range of the order of atomic units, the Born expansion quickly converges [3] (see, however, Ref. [5]). In fact, extensive *S*-matrix calculations employing a short-range or even zero-range potential qualitatively reproduce the main features of high-order above-threshold ionization (ATI) of neutral atoms and molecules [4]. For photodetachment of negative ions, even quantitative agreement for the spectrum from low to high energy has been achieved [8]. However, there are cases where the long-range Coulomb potential, instead of a short-range or zero-range model potential, has to be adopted to better reproduce the experimental observations, e.g., the height of the plateau of the photoelectron spectrum [9]. If so, the higher-order term may be larger than the lowest-order term. One prominent example is the theoretical explanation of the low-energy structure (LES) [10,11] in the photoelectron spectrum at long wavelengths, which cannot be accounted for by the lowest-order *S*-matrix theory (i.e., the SFA). The second order reproduces the effect qualitatively and even semiquantitatively if an unscreened Coulomb potential is adopted. By considering the depletion of the atomic ground state due to

*These authors contributed equally to this work.
†charlywing@wipm.ac.cn
‡chen_jing@iapcm.ac.cn
§xjliu@wipm.ac.cn

the applied laser field, technical problems related to the divergence of the Coulomb forward-scattering amplitude are remedied [7,12]. However, there are indications that the third-order term, which includes one more interaction between the electron and the long-range ionic potential, overwhelms the second-order term so that the convergence of the expansion becomes questionable. Hence, the validity of these calculations remains a problem. Nevertheless, it is conceivable that the second-order term provides an effective theory for the physical process.

Another example that inevitably incorporates the long-range Coulomb potential is RSE in an intense laser field [13–17], which is explained by a semiclassical recapture [14] or "frustrated tunneling ionization" (FTI) mechanism [15]. It is relevant to various significant issues, such as coherent extreme-ultraviolet emission [18], acceleration of neutral atoms [13], and many more. Recently, an *S*-matrix theory for the field-induced dynamics of highly excited Rydberg states has been formulated which proposed a coherent-capture picture of RSE [19–21]. It illustrates the close connection between RSE below and ATI, especially the LES, above the continuum limit [19].

In this paper, we use this theory to address a particularly conspicuous phenomenon, the oscillation [22–24] as a function of the laser intensity of the ratio of Rydberg excitation over ionization and the pertinent scaling of the oscillation period and the intensity-averaged ratio as a function of the laser wavelength. We take the argon atom as an example. The experimental data that we report and present exhibit excellent agreement with the results of our theory. While the question of the convergence of the Born-series expansion of the *S*-matrix amplitude remains open, our results allow us to state that for RSE (equally well as for ATI) the first two terms of the Born series provide an effective theory that describes the observations very well.

II. EXPERIMENTAL METHOD

In our experiments, wavelength-tunable femtosecond laser pulses are generated by an optical parametric amplifier (TOPAS-C, Light Conversion, Inc.) pumped by a commercial Ti:sapphire laser system (Legend, Coherent, Inc.), which produces 30 fs laser pulses at 800 nm. The duration of the laser pulse from TOPAS-C is ∼35 fs for the signal pulse (for 1300 and 1500 nm) and ∼55 fs for the idler pulse (for 1800 nm). Before being focused into the vacuum chamber, the pulse energy from the optical parametric amplifier can be varied by means of an achromatic half-wave plate followed by a polarizer. As shown in Fig. 1, a collimated supersonic atomic beam of Ar intersects the laser beam at the focal spot. The ion and neutral-atom signals produced at the interaction point are registered by a homemade spectrometer dedicated to investigate the RSE process [19,21]. At the interaction spot, a pulsed and a constant electric field [see Fig. 1(a)] are applied to the first two electrodes and the third electrode is grounded. With careful choice of the duration (9.0 μs) of the pulsed fields and the delay time (1.2 μs) with respect to the laser pulse, the singly charged ions Ar^+ and the neutral atoms Ar^* with $n \leqslant 75$ can be measured simultaneously. During the data acquisition, the laser pulse energy is recorded shot by shot by

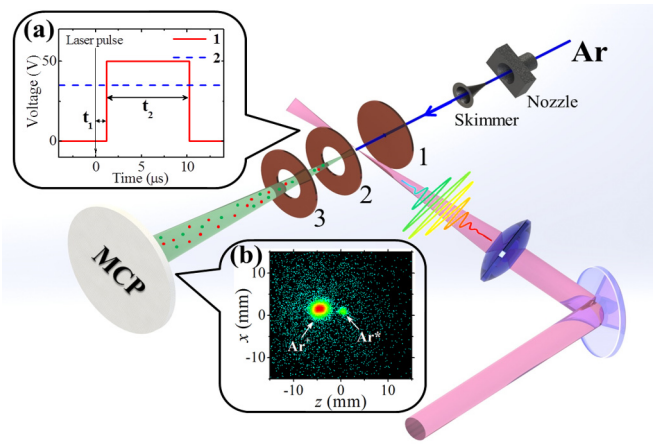

FIG. 1. Sketch of the experimental setup. A focused linearly polarized laser beam intersects a collimated supersonic beam of Ar in between electrode plates 1 and 2. The electric voltages which are applied to plates 1 and 2 are shown in (a), where $t_1 = 1.2\,\mu$s and $t_2 = 9.0\,\mu$s. Plate 3 is grounded. Panel (b) shows the image of singly charged ions Ar^+ and excited atoms Ar^* spatial distributions on the detector.

a photodiode equipped with a homemade integration circuit. In the off-line analysis, only the data with pulse energies in a small range are chosen to obtain the yields at each intensity. In this way, the laser intensity fluctuations can be well reduced for the experimental data (see Refs. [19,21] for details). The laser intensity has been calibrated with the 10-U_p cutoff (U_p is the ponderomotive energy of the laser field) of the above-threshold ionization spectra of Ar [25].

III. *S*-MATRIX THEORY

In *S*-matrix theory, the RSE probability with the electron in the initial state $|\Psi_i\rangle$ is given by $P = \sum_{nlm} |M_{nlm}|^2$, with M_{nlm} the exact RSE amplitude. To first order in the Born expansion, it is [20]

$$M_{nlm}^{(1)} = (-i)^2 \int_{-\infty}^{\infty} dt_c \int_{-\infty}^{t_c} dt_i \int d^3\mathbf{k} \langle \Psi_{nlm}^d(t_c) | V | \Psi_{\mathbf{k}}^{(V)}(t_c) \rangle \times \langle \Psi_{\mathbf{k}}^{(V)}(t_i) | H_I(t_i) | \Psi_i(t_i) \rangle. \quad (1)$$

We approximate the final field-dressed Rydberg state by

$$\Psi_{nlm}^d(\mathbf{r}, t) = \psi_{nlm}(\mathbf{r}) e^{-iE_n t} e^{i\mathbf{A}(t)\cdot\mathbf{r}} e^{-i\int_{-\infty}^{t} dt' \mathbf{A}^2(t')/2}, \quad (2)$$

which approximately satisfies the time-dependent Schrödinger equation [20]. Here, the state $\psi_{nlm}(\mathbf{r})$ is a field-free Rydberg state corresponding to the energy level $E_n = -1/(2n^2)$, and the principal, angular-momentum, and magnetic quantum numbers are n, l, and m, respectively. The kets $|\Psi_{\mathbf{k}}^{(V)}(t)\rangle$ denote the intermediate Volkov states. In length gauge, $H_I(t) = \mathbf{r} \cdot \mathbf{E}(t)$, with the linearly polarized electric field $\mathbf{E}(t) = E_0 \sin \omega t \hat{\mathbf{e}}_z$ and the vector potential $\mathbf{A}(t) = -\int_{-\infty}^{t} \mathbf{E}(\tau) d\tau$, where E_0 is the peak amplitude. The Coulomb potential is denoted by $V(\mathbf{r}) = -1/|\mathbf{r}|$. The initial state $\Psi_i(\mathbf{r}, t_i)$ is described by a $3p_z$ Slater-type orbital of the Ar atom. The structure of the core plays no role since it has hardly any overlap with the region where the wave

function of the Rydberg state is mainly located. Therefore, in our calculation we use the wave functions of the hydrogen atom to approximate the Rydberg states of Ar. Indeed, as demonstrated earlier [19–21], the experimental data for Ar and Xe can be well reproduced if the wave functions of hydrogen are employed as the final state.

To second order, the excitation amplitude, which includes rescattering, is [19]

$$M_{nlm}^{(2)} = (-i)^3 \int_{-\infty}^{\infty} dt_r \int_{-\infty}^{t_r} dt_i \int_{t_r}^{\infty} dt_c \int d^3\mathbf{p} \int d^3\mathbf{k} \times \langle \Psi_{nlm}^{d}(t_c) | V | \Psi_{\mathbf{p}}^{(V)}(t_c) \rangle \langle \Psi_{\mathbf{p}}^{(V)}(t_r) | V | \Psi_{\mathbf{k}}^{(V)}(t_r) \rangle \times \langle \Psi_{\mathbf{k}}^{(V)}(t_i) | H_I(t_i) | \Psi_i(t_i) \rangle, . \quad (3)$$

where t_i, t_r, and t_c denote the instants of ionization, rescattering, and capture where $t_c > t_r > t_i$. The momenta after and before rescattering are $\mathbf{p}$ and $\mathbf{k}$. The calculational details of Eqs. (1) and (3) can be found in Refs. [20] and [19], respectively.

For ionization, the corresponding terms of the S-matrix expansion are

$$M_{\mathbf{p}}^{(1)} = -i \int_{-\infty}^{\infty} dt_i \langle \Psi_{\mathbf{p}}^{(V)}(t_i) | \mathbf{r} \cdot \mathbf{E}(t_i) | \Psi_i(t_i) \rangle \quad (4)$$

and

$$M_{\mathbf{p}}^{(2)} = (-i)^2 \int_{-\infty}^{\infty} dt_r \int_{-\infty}^{t_r} dt_i \int d^3\mathbf{k} \langle \Psi_{\mathbf{p}}^{(V)}(t_r) | V | \Psi_{\mathbf{k}}^{(V)}(t_r) \rangle \times \langle \Psi_{\mathbf{k}}^{(V)}(t_i) | \mathbf{r} \cdot \mathbf{E}(t_i) | \Psi_i(t_i) \rangle, \quad (5)$$

which are often referred to as the SFA [1–3] and the "improved SFA" (ISFA) [4], respectively. The second-order amplitudes (3) and (5) suffer from convergence problems if forward Coulomb scattering is taken into account. In this paper, the depletion of the ground state is introduced to eliminate the divergence that originates from forward scattering due to the long range of the Coulomb potential [7]. It is important to mention that the ionization yield has to be calculated by the sum of the two terms considered in the expansion. In contrast, for the RSE yield it is sufficient to consider only the highest-order term (here the second order) because the contributions of all lower-order terms vanish due to diffusion of the continuum wave packet in the intermediate state [19,20].

IV. RESULTS AND DISCUSSION

In Figs. 2(a)–2(d), the measured intensity dependence of the ratio of the yields of Ar^* over Ar^+ at 800, 1300, 1500, and 1800 nm as well as the calculation via the second-order term (3) of the S-matrix expansion are presented. The ratio exhibits a pronounced oscillatory structure as a function of the laser intensity. According to Ref. [19], for 800 nm the oscillation can be attributed to channel closings [20,21], while at the longer wavelengths the interference of the contributions of different capture trajectories is responsible for the oscillatory structure observed. The same trajectories also contribute to the LES peaks of different orders. So, in Fig. 3(a) we plot the wavelength dependence of the oscillation period from 1300 to 1800 nm. It shows a monotonically decreasing trend with increasing laser wavelength. A curve of $\lambda^{-1.2}$ can well

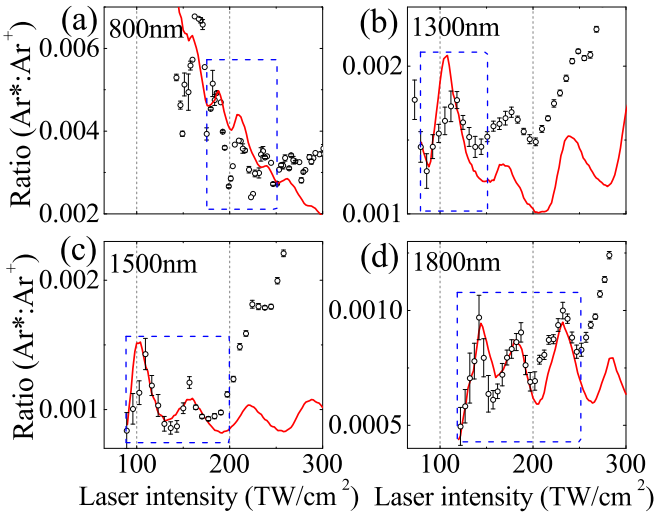

FIG. 2. The measured (circles) and calculated (lines) ratio of the yields of Ar^* over Ar^+ as a function of intensity at (a) 800, (b) 1300, (c) 1500, and (d) 1800 nm.

match the measured curve, in agreement with the calculation of Ref. [19]. Moreover, the ratio is highest at 800 nm and decreases with increasing laser wavelength as shown in Fig. 3(b). The wavelength dependence of the calculated intensity-averaged ratio of Ar^* over Ar^+ based on the quantum model is also presented in Fig. 3(b). We notice very good agreement between the measurements and the second-order calculation. On the other hand, the ratio calculated by only the first-order term decreases much more slowly with wavelength than the experimental result.

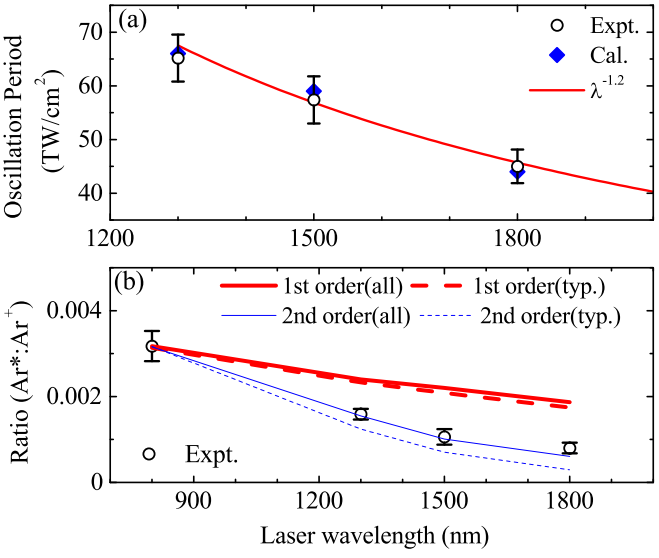

FIG. 3. (a) The wavelength dependence of the period of oscillations of the yield ratios in Figs. 2(b)–2(d). (b) The wavelength dependence of the intensity-averaged ratio of the Ar^* over Ar^+ yield. The blue dashed rectangles in Figs. 2(a)–2(d) indicate the intensity ranges, which are employed to obtain the measured averaged ratios of (b). The dashed lines in (b) represent the results of calculations where only the typical trajectories shown in Fig. 5 are considered, while the solid lines represent the calculations where all trajectories are considered. See the text for more details.

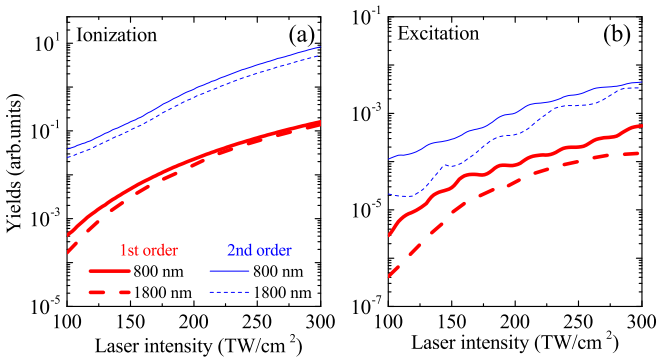

FIG. 4. The intensity dependence of (a) ionization and (b) excitation yields for Ar calculated by the first (thick red) and the second (thin blue) order terms at 800 nm (solid lines) and 1800 nm (dashed lines).

In Fig. 4, the intensity dependence of the ionization [Eqs. (4) and (5)] and excitation [Eqs. (1) and (3)] yields of Ar calculated by the first- and second-order terms at 800 nm and 1800 nm is presented. One prominent feature is that, for both ionization and RSE, the yields calculated by the second-order terms exceed those of the first-order terms by more than one order of magnitude throughout the intensity range considered. This can be attributed to the large forward-scattering cross section of the ion's long-range Coulomb potential [7]. It can be expected that the third-order term will again be larger than the second-order term, so that the convergence of the expansion is put into question. However, considering that we only compare the wavelength dependence of the *ratio* between the excitation and ionization yields with the experimental data, the apparent divergence of the transition amplitude for higher orders may not affect this ratio, since the divergence due to the forward-scattering of the photoelectron off the long-range Coulomb potential will cancel in the aforementioned ratio provided the scattering is considered to the same order (in the present calculation, it is taken into account once). Furthermore, according to Ref. [19], the oscillation in the intensity dependence of the RSE yield in a long-wavelength laser field is due to the interference between trajectories contributing to different orders of the LES, which is solely dependent on the relative phase between these trajectories and will not be affected by the collision between the electron and ionic potential, implying that the high-order terms have no effect on the oscillations. Therefore, we propose that truncating the Born series at the second-order term, which corresponds to the first-order Rutherford term in the field-free Coulomb scattering, can provide an effective theory for the description of the dynamics of atoms in an intense laser field. This hypothesis can be checked by experiment and is solidly supported by the results displayed in Figs. 2 and 3. The LES, which is attributed to the interaction between the photoelectron and ionic Coulomb potential [11,26], can also be well described by the second-order term of the S-matrix expansion [7].

In addition, Fig. 4(a) shows that the ionization yields calculated by both the first and second order drop by about 50% when the wavelength increases from 800 nm to 1800 nm. In contrast, according to Fig. 4(b) both the first- and the second-order contributions to the RSE probability decrease much faster with increasing wavelength, and the second-order

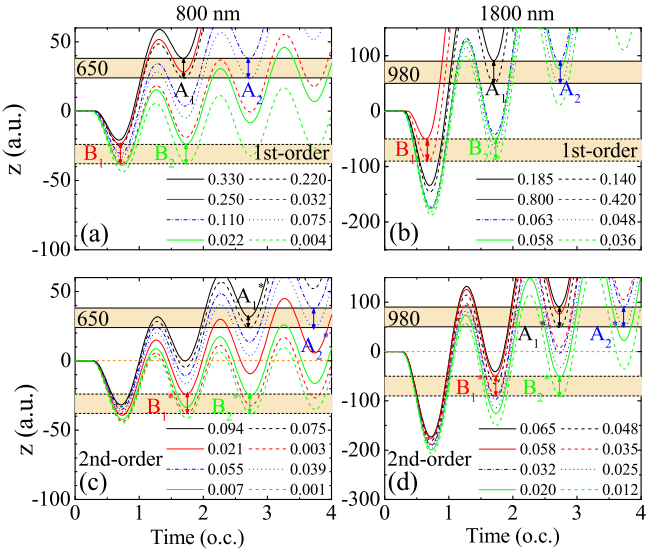

FIG. 5. Typical trajectories that are relevant for the coherent capture process into the Rydberg states 650 (left column) and 980 (right column). The horizontal shaded regions indicate the spatial regions where the photoelectron wave packets are captured into the corresponding Rydberg state. The final energy of each trajectory in units of the ponderomotive energy U_p is indicated in each panel. Panels (a) and (b) display simple-man trajectories that contribute to the first-order term (without rescattering), while panels (c) and (d) show those that contribute to the second order, having undergone rescattering once. Short vertical arrows in the panels labeled by a capital letter identify the energy ranges where capture happens in the low-energy regime. The wavelength is 800 nm for the left column and 1800 nm for the right column. See the text for details.

term drops even more quickly than the first-order term in the low-intensity region (below $2 \times 10^{14}\,\mathrm{W/cm^2}$), in good agreement with the experimental data [as shown in Fig. 3(b)].

In what follows, we will discuss typical simple-man trajectories of electrons that dominantly contribute in the parameter regime we consider. The goal is to understand the different wavelength dependence of the first- and the second-order terms, and the relationship between RSE on the one hand and ATI, especially the LES, on the other. Simple-man trajectories have the electron starting after tunneling at the origin with zero initial velocity and subsequently evolving in the external field [12]. The typical trajectories that contribute significantly to the excitation yields of the first-order term (1) are depicted in Figs. 5(a) (for 800 nm) and 5(b) (for 1800 nm). The first-order amplitude contains the binding potential $V(\mathbf{r})$ only once, and this matrix element mediates the transition into the final Rydberg state. In contrast, the second-order term (3) contains the binding potential twice, which allows the electron on the corresponding trajectory first to rescatter before it recombines into the Rydberg state. Such trajectories are depicted in Figs. 5(c) (for 800 nm) and 5(d) (for 1800 nm). The shaded brown regions in Fig. 5 indicate the spatial regions where the wave functions of the relevant Rydberg states have their highest density so that the electrons have the highest probability of being captured. These are $n = 6$, $l = 5$, $m = 0$ and $n = 9$, $l = 8$, $m = 0$, which will be referred to by (650) and (980) in the figure and below. If an electron trajectory

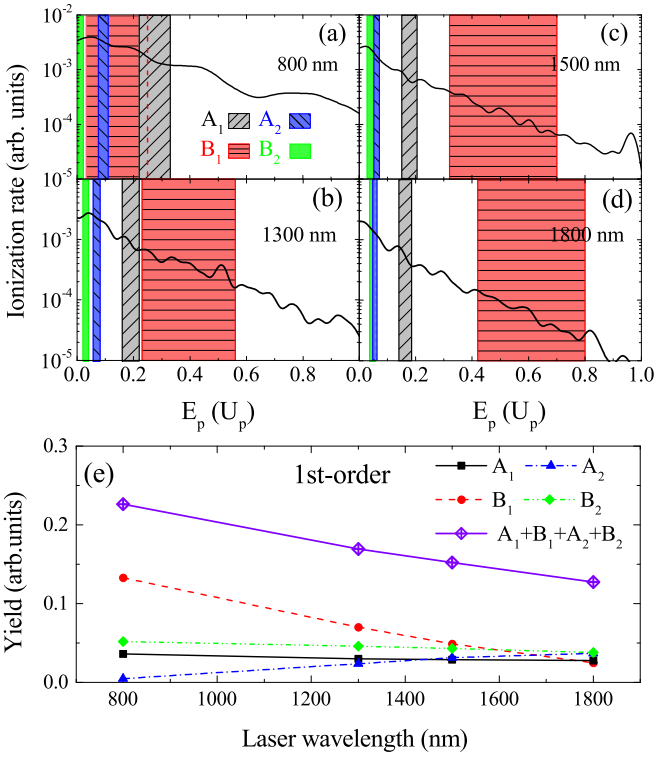

FIG. 6. Low-energy PES (black lines) calculated by the first-order term [Eq. (4)] of S-matrix theory at (a) 800 nm, (b) 1300 nm, (c) 1500 nm, and (d) 1800 nm. The stripes labeled by A_i and B_i identify the energy regions for the first-order coherent recapture process using the same letters as in Figs. 5(a) and 5(b). (e) Wavelength dependence of the RSE yields calculated by integration over the energy ranges in the PES specified in (a)–(d).

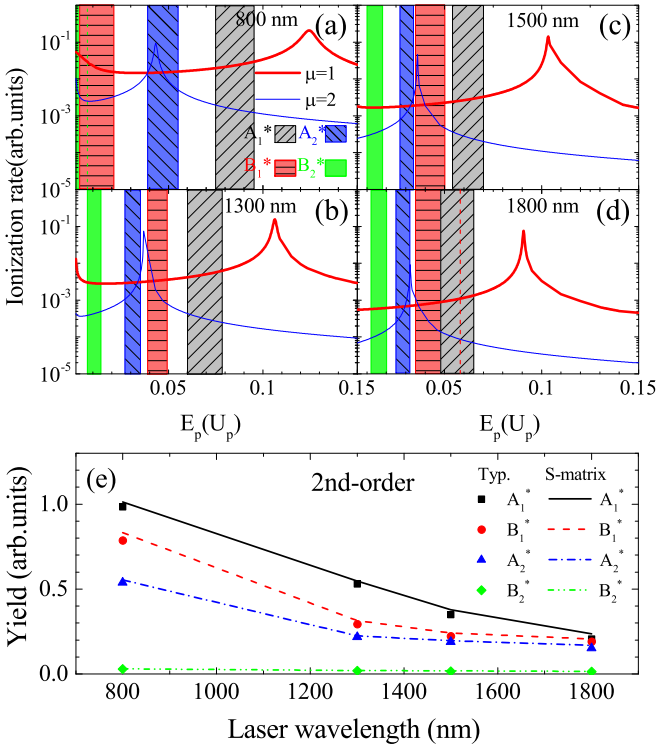

FIG. 7. Low-energy photoelectron kinetic energy spectra calculated by the second-order term [Eq. (5)] (thick red line for $\mu = 1$ and thin blue line for $\mu = 2$) of S-matrix theory at (a) 800 nm, (b) 1300 nm, (c) 1500 nm, and (d) 1800 nm. The stripes labeled A_i^* and B_i^* identify the energy regions for the second-order coherent recapture process using the same letters as in Figs. 5(c) and 5(d). (e) Wavelength dependence of the RSE yields calculated by integration over the energy ranges in the PES shown in (a)–(d) and those calculated by the second-order term of the S-matrix theory.

reaches a shaded brown region with small kinetic energy or, in other words, if it turns around inside this region, then the electron is considered to be captured by the corresponding Rydberg state [19,20].

Capture may occur at $z > 0$ or $z < 0$. In Fig. 5, we label the first case by A_i (A_i^*) and the second by B_i (B_i^*) for the first-order (second-order) term. The subscript i enumerates the capture events according to increasing capture time. For example, the capture event indicated by A_1 during the interval $(1.5, 2)T$ [see Fig. 5(a)] contributes to the first-order term, while the one indicated by A_1^* during the time interval $[2.5T, 3T]$ contributes to the second-order term because it includes low-energy rescattering during $[1.5T, 2T]$ [see Fig. 5(c)]. Note that the same simple-man trajectory may contribute to the first- and the second-order (and, possibly, higher-order) terms, but with different capture times.

On the other hand, electrons following these trajectories can also reach the continuum and contribute to the LES. In Figs. 6 and 7, the low-energy photoelectron kinetic-energy spectra (PES) calculated from the first-order term (4) and the second-order term (5) for four different wavelengths (800, 1300, 1500, and 1800 nm) are presented together with the final-energy ranges of the typical capture trajectories that are shown in Fig. 5 for the wavelengths of 800 and 1800 nm. For 1300 and 1500 nm, the main contributions to RSE come from the states of (760) and (870), respectively. There is consensus [12,26] that the LES is the result of electron-energy bunching in laser-driven elastic forward scattering. Hence, the LES cutoff energies correspond to trajectories that turn around at the position $z = 0$ of the ion, represented by the horizontal dashed orange lines in Figs. 5(c) and 5(d) [12]. The relevant trajectories can be classified by an index μ, which is closely related to the travel time of the photoelectron between ionization and the forward-scattering event (a detailed introduction of the index can be found in Ref. [12]). The second-order PES spectra in Figs. 7(a)–7(d) exhibit distinct peaks at the electron energies of about $0.1U_p$ ($\mu = 1$) and $0.03U_p$ ($\mu = 2$), which correspond to the energies of the lowest two orders of LES. As expected, the first-order contribution to the photoelectron yield (see Fig. 6, no rescattering) drops rather smoothly with respect to the electron energy, while the second-order contribution (Fig. 7, with rescattering) depends more strongly on the energy and exhibits the LES peaks.

The low-energy PES and the energy regions corresponding to the captured trajectories, as shown in Figs. 6 and 7, can help in understanding the relation between the contributions of the first-order and the second-order terms and, especially, their wavelength scaling. Namely, as shown in Ref. [19], the yields of the photoelectrons that correspond to the final energies of the recapture trajectories are closely related to the RSE

yields. This illustrates the strong influence of the LES and the Coulomb potential on the RSE yields. The shaded stripes that are labeled by A_i (A_i^*) and B_i (B_i^*) in Fig. 6 (Fig. 7) denote the final-energy ranges for the recapture trajectories calculated by the first-order term (1) [second-order term (3)] of S-matrix theory. The ranges of trajectories corresponding to these energy ranges are labeled by the same letters as in Fig. 5. For each term, the RSE yield of the trajectories denoted by the letter A or B is proportional to the photoelectron yield for the energy range denoted by the same letter. A very important feature can be observed in Figs. 6 and 7: the ranges A_i and A_i^*, which correspond to capture at $z > 0$, shift to lower photoelectron energies with increasing wavelength, while the ranges B_i and B_i^*, which correspond to capture at $z < 0$, shift to higher energies.

The feature mentioned above can be comprehended by the analysis below. In Fig. 5, the higher the final energy of a trajectory, the later is its instant of ionization (this is hard to see on the scale of the figure). When the final energy of a trajectory decreases, which corresponds to earlier time of ionization, the position along its trajectory where the electron turns around, to be referred to as a U-turn point in the following, shifts downwards (in the negative direction of z). Note that, with increasing wavelength, the quiver amplitude of the electron, which is proportional to λ^2, increases faster than the spatial capture region, which increases linearly with wavelength; e.g., the wave functions of the states (650), (760), (870), and (980) are centered at 31, 51, 58, and 70 a.u., respectively. Thus, the ranges of capture in the positive (negative) direction of z move towards (away from) $z = 0$, giving rise to an earlier (later) tunneling instant with increasing wavelength, with the consequence of a shift of the energy intervals A_i and A_i^* (B_i and B_i^*) towards lower (higher) energies [as can be seen in Figs. 6(a)–6(d) and 7(a)–7(d)]. In addition, the widths of the capture regions (the shaded brown regions in Fig. 5) increase almost linearly (with a wavelength scaling of $\lambda^{1.1}$) [19]. In contrast, the distance between the U-turn points of two trajectories with specific tunneling phases is proportional to $dz/d\phi_0 \propto \lambda^2 \sin\phi_0$ [for the laser field $\mathbf{E}(t) = \mathbf{E_0}\cos\omega t$], where z is the position of the U-turn point and ϕ_0 the ionization phase of the electron. On the other hand, we have $dE_k/d\phi_0 = 2U_p \sin 2\phi_0$, where E_k is the final kinetic energy. These two derivatives increase with ϕ_0 for small ϕ_0 as considered here. The combined effect of these factors will make the widths of the capture ranges in the PES change obviously in some cases when the ranges shift significantly. As shown in Figs. 6 and 7, the regions A_1 and A_2^* shrink noticeably with increasing wavelength, especially when the wavelength increases from 800 nm to 1300 nm, while the region B_1 expands significantly when the wavelength increases from 800 nm to 1300 nm and only slightly thereafter.

The RSE yields of the energy ranges labeled by A_i, B_i, A_i^*, and B_i^* are plotted in Fig. 6(e) for the first-order term and in Fig. 7(e) for the second-order term as functions of the wavelength. For the first-order term, the yields of the ranges B_i decrease with wavelength since they shift to higher energies and the photoelectron yield drops with kinetic energy [see Figs. 6(a)–6(d)]. It is worth noting that the range B_2 drops only slightly because it is very close to zero and the shift of its position is small when the wavelength changes. The ranges A_i shift to the lower energy region with increasing wavelength, so their yields tend to increase with wavelength. However, the yield of the range A_1 remains almost unchanged because its width strongly shrinks.

For the second-order term, the range A_1^*, which makes the largest contribution to the RSE yield, shifts away from the highest LES peak with increasing wavelength. Therefore, its yield drops quickly. The range A_2^* shifts to lower energy but stays near the peak of the second-order LES. However, since its width shrinks with increasing wavelength as mentioned above, its yield first decreases quickly when the wavelength increases from 800 nm to 1300 nm and slowly thereafter when the wavelength further increases. The range B_1^* keeps moving towards the first-order LES peak. However, the corresponding PES yield drops quickly with increasing wavelength, especially when the wavelength increases from 800 nm to 1300 nm, so its yield follows a similar curve as the range A_2^*. This fast drop of the PES in a regime far away from the LES peak is due to the fact that the LES becomes more pronounced with increasing wavelength. For the same reason, the yield of the range B_2^* also decreases with wavelength, but its contribution is negligible since it is far away from the peak of the second-order LES.

The combined contribution of all these ranges is also shown in Fig. 3(b) and labeled by "1st order(typ.)" and "2nd order(typ.)." Obviously, these trajectories make the most significant contributions, and the calculations for only these trajectories are almost coincident with the complete S-matrix calculations, which consider all trajectories. According to the above analysis, the faster decrease of the RSE yield of the second-order term compared with the first-order term can be attributed to the marked difference between the smooth and monotonic PES from the SFA theory and the pronounced peaks of the LES in the PES, which are due to the Coulomb potential being included in the second-order term. The difference between the two spectra and the underlying capture dynamics (in the second-order term, the main contribution comes from capture events occurring after the electron experienced forward scattering upon the ionic potential) not only alters the relative contributions from different capture ranges (the most important contribution comes from the range B_1 for the first-order term and A_1^* for the second order), but, more importantly, it also changes the wavelength dependence of the yields of the individual capture ranges. For the first-order term, the yields of the capture ranges in the positive direction increase with wavelength, while, for the second-order term, the yields in both directions decrease with wavelength, resulting in the different scaling laws of the RSE wavelength dependence in the two cases.

V. CONCLUSION

In conclusion, we have performed a joint experimental and theoretical investigation of the wavelength dependence of the processes of strong-field atomic ionization and Rydberg-state excitation. We found that the wavelength scaling law of the measured ratio of Ar^* over Ar^+ and the period of its oscillation with respect to the laser intensity can be well reproduced by the second-order term of the Born series of the S matrix, but not by the lowest-order term (SFA). Our work strongly

supports the conjecture that the second-order term of the Born series of the S matrix can be envisioned to provide an effective theory for the intense-laser–atom interaction. In analogy to the Born expansion of the field-free Coulomb-scattering amplitude, this may provide a pivotal milestone on the way to a comprehensive quantum theory for the atomic dynamics in strong laser fields.

ACKNOWLEDGMENTS

We thank Y. Q. Xu, H. Y. Sun, C. Z. Wan, Y. Wang, and Q. F. Chen for technical support of the laser system, electronic devices, and vacuum system. This work is supported by the National Key Research and Development Program of China (Grant No. 2019YFA0307700), the National Natural Science Foundation of China (Grants No. 11834015, No. 11974383, No. 12121004, No. 12147117, No. 12104465, and No. U21A20435), the China Postdoctoral Science Foundation (Grant No. 2019M662752), the Youth Innovation Promotion Association CAS (Grant No. 2021328), the Science and Technology Department of Hubei Province (Grants No. 2019CFA035 and No. 2020CFA029), and the K. C. Wong Education Foundation.

[1] L. V. Keldysh, Ionization in the field of a strong electromagnetic wave, Sov. Phys. JETP. **20**, 1307 (1965).

[2] F. H. M. Faisal, Multiple absorption of laser photons by atoms, J. Phys. B: At. Mol. Phys. **6**, L89 (1973).

[3] H. R. Reiss, Effect of an intense electromagnetic field on a weakly bound system, Phys. Rev. A **22**, 1786 (1980).

[4] W. Becker, F. Grasbon, R. Kopold, D. B. Milošević, G. G. Paulus, and H. Walther, Above-threshold ionization: From classical features to quantum effects, Adv. At. Mol. Opt. Phys. **48**, 35 (2002).

[5] A. Galstyan, O. Chuluunbaatar, A. Hamido, Y. V. Popov, F. Mota-Furtado, P. F. O'Mahony, N. Janssens, F. Catoire, and B. Piraux, Reformulation of the strong-field approximation for light-matter interaction, Phys. Rev. A **93**, 023422 (2016).

[6] B. Piraux, A. Galstyan, Yu. V. Popov, F. Mota-Furtado, and P. F. O'Mahoney, Iterative treatment of the Coulomb potential in laser-atom interaction, Eur. Phys. J. D **75**, 196 (2021).

[7] L. Guo, S. S. Han, X. Liu, Y. Cheng, Z. Z. Xu, J. Fan, J. Chen, S. G. Chen, W. Becker, C. I. Blaga, A. D. DiChiara, E. Sistrunk, P. Agostini, and L. F. DiMauro, Scaling of the Low-Energy Structure in Above-Threshold Ionization in the Tunneling Regime: Theory and Experiment, Phys. Rev. Lett. **110**, 013001 (2013).

[8] A. Gazibegović-Busuladžić, D. B. Milošević, W. Becker, W. Bergues, H. Hultgren, and I. Y. Kiyan, Electron Rescattering in Above-Threshold Photodetachment of Negative Ions, Phys. Rev. Lett. **104**, 103004 (2010).

[9] D. B. Milošević and F. Ehlotzky, Influence of screening of the Coulomb potential on the plateau in above-threshold ionization, Phys. Rev. A **57**, 5002 (1998).

[10] C. I. Blaga, F. Catoire, P. Colosimo, G. G. Paulus, H. G. Muller, P. Agostini, and L. F. DiMauro, Strong-field photoionization revisited, Nat. Phys. **5**, 335 (2009).

[11] W. Quan, Z. Lin, M. Wu, H. Kang, H. Liu, X. Liu, J. Chen, J. Liu, X. T. He, S. G. Chen, H. Xiong, L. Guo, H. Xu, Y. Fu, Y. Cheng, and Z. Z. Xu, Classical Aspects in Above-Threshold Ionization with a Midinfrared Strong Laser Field, Phys. Rev. Lett. **103**, 093001 (2009).

[12] W. Becker, S. P. Goreslavski, D. B. Milošević, and G. G. Paulus, Low-energy electron rescattering in laser-induced ionization, J. Phys. B: At. Mol. Opt. Phys. **47**, 204022 (2014).

[13] U. Eichmann, T. Nubbemeyer, H. Rottke, and W. Sandner, Acceleration of neutral atoms in strong short-pulse laser fields, Nature (London) **461**, 1261 (2009).

[14] W. Bing-Bing, L. Xiao-Feng, F. Pan-Ming, C. Jing, and L. Jie, Coulomb potential recapture effect in above-barrier ionization in laser pulses, Chin. Phys. Lett. **23**, 2729 (2006).

[15] T. Nubbemeyer, K. Gorling, A. Saenz, U. Eichmann, and W. Sandner, Strong-Field Tunneling without Ionization, Phys. Rev. Lett. **101**, 233001 (2008).

[16] U. Eichmann, A. Saenz, S. Eilzer, T. Nubbemeyer, and W. Sandner, Observing Rydberg Atoms to Survive Intense Laser Fields, Phys. Rev. Lett. **110**, 203002 (2013).

[17] H. Zimmermann, J. Buller, S. Eilzer, and U. Eichmann, Strong-Field Excitation of Helium: Bound State Distribution and Spin Effects, Phys. Rev. Lett. **114**, 123003 (2015).

[18] H. Yun, J. H. Mun, S. I. Hwang, S. B. Park, I. A. Ivanov, C. H. Nam, and K. T. Kim, Coherent extreme-ultraviolet emission generated through frustrated tunnelling ionization, Nat. Photon. **12**, 620 (2018).

[19] M. Liu, S. Xu, S. Hu, W. Becker, W. Quan, X. Liu, and J. Chen, Electron dynamics in laser-driven atoms near the continuum threshold, Optica **8**, 765 (2021).

[20] S. L. Hu, X. L. Hao, H. Lv, M. Q. Liu, T. X. Yang, H. F. Xu, M. X. Jin, D. J. Ding, Q. G. Li, W. D. Li, W. Becker, and J. Chen, Quantum dynamics of atomic Rydberg excitation in strong laser fields, Opt. Express **27**, 31629 (2019).

[21] S. Xu, M. Liu, S. Hu, Z. Shu, W. Quan, Z. Xiao, Y. Zhou, M. Wei, M. Zhao, R. Sun, Y. Wang, L. Hua, C. Gong, X. Lai, J. Chen, and X. Liu, Observation of a transition in the dynamics of strong-field atomic excitation, Phys. Rev. A **102**, 043104 (2020).

[22] Q. Li, X. M. Tong, T. Morishita, H. Wei, and C. D. Lin, Fine structures in the intensity dependence of excitation and ionization probabilities of hydrogen atoms in intense 800-nm laser pulses, Phys. Rev. A **89**, 023421 (2014).

[23] B. Piraux, F. Mota-Furtado, P. F. O'Mahony, A. Galstyan, and Y. V. Popov, Excitation of Rydberg wave packets in the tunneling regime, Phys. Rev. A **96**, 043403 (2017).

[24] H. Zimmermann, S. Patchkovskii, M. Ivanov, and U. Eichmann, Unified Time and Frequency Picture of Ultrafast Atomic Excitation in Strong Laser Fields, Phys. Rev. Lett. **118**, 013003 (2017).

[25] F. Grasbon, G. G. Paulus, H. Walther, P. Villoresi, G. Sansone, S. Stagira, M. Nisoli, and S. DeSilvestri, Above-Threshold Ionization at the Few-Cycle Limit, Phys. Rev. Lett. **91**, 173003 (2003).

[26] A. Kästner, U. Saalmann, and Jan M. Rost, Electron-Energy Bunching in Laser-Driven Soft Recollisions, Phys. Rev. Lett. **108**, 033201 (2012).